Spectroscopic investigation of light-emitting porous silicon photoetched in aqueous HF/I_2 solution

Sadao Adachi and Mitsuru Oi
Department of Electronic Engineering, Faculty of Engineering, Gunma University, Kiryu-shi, Gunma 376-8515, Japan

(Received 8 July 2007; accepted 23 July 2007; published online 18 September 2007)

The optical properties of porous silicon (PSi) photoetched in aqueous HF/I_2 solution are investigated using spectroellipsometry (SE), electroreflectance (ER), photovoltage (PV), photoconductivity (PC), photoluminescence (PL), and Fourier transform infrared (FTIR) spectroscopy. The PSi layers were formed in a HF/I_2 solution on *n*-Si substrates under Xe lamp illumination. The SE $\varepsilon(E)$ and related data show an interference oscillation in the region below $E \sim 3$ eV, where the PSi material is nearly transparent. The PV and PC spectra reveal three individual peaks *A*, *B*, and *C* at ~1.2, ~1.7, and ~2.5 eV, respectively, arising from the PSi layer itself. Peak *C* is also observed in the ER spectrum, together with a broadened E_1 peak at ~3.4 eV. Change in the fundamental-absorption-edge nature (E_g^X) from the indirect gap in crystalline silicon to the quasidirect gap in PSi is found in the PV and PC spectra. The PL spectrum shows a broad peak at ~2.0 eV(*B*). Peaks *A*, *B*, and *C* observed in the PSi layer may originate from the nondirect optical transitions at and above the lowest absorption edges E_g^X (*A* and *B*) and E_g^L (*C*). The quantum-mechanical size effect, i.e., a relaxation of the momentum conservation, makes possible the nondirect or quasidirect transitions at and above E_g^X and E_g^L in porous materials. The FTIR data support that the PL emission is due to the surface-sensitive quantum confinement effect. © *2007 American Institute of Physics*. [DOI: 10.1063/1.2778745]

I. INTRODUCTION

The optical properties of porous and nanocrystalline silicon-based light-emitting structures have attracted particular interest both from scientific and technological points of view.[1] An important challenge pervading solid-state physics is the problem of understanding the optical properties of a material in terms of its fundamental properties. Quantum confinement is the first model proposed to explain visible photoluminescence (PL) from porous silicon (PSi).[2] Afterwards, many other alternative models were proposed: (1) hydrogenated amorphous silicon model, (2) surface hydride model, (3) defect model, (4) siloxene model, and (5) surface state model.[1,3] Except for the quantum confinement model, all the others assume an extrinsic origin for PSi luminescence.

Most PSi layers have been formed by conventional anodic etching in a HF-based electrolyte.[1,3] The requirements of a backcontact electrode and electronic circuits are the demerits of anodic etching. The PSi layers can also be formed by simply immersing a Si wafer in a HF-based solution without (stain etching) or with light illumination (photoetching). The first report of a light-emitting PSi layer obtained by stain etching came from Sarathy *et al.*[4] who used an aqueous HF/HNO_3 solution. Some authors also demonstrated the formation of a luminescent PSi by photoetching in HF-based solutions under He−Ne laser illumination.[5–9] More recently, we reported the formation of luminescent PSi layers by photoetching in a HF solution containing some oxidizing agents, such as KIO_3,[10] I_2,[11] and $FeCl_3$,[12] and using an incoherent light source (Xe lamp). This method enabled to obtain a large ($\geq 20 \times 20$ mm^2), homogeneous PSi layer in a very short time (<10 min).[10–12] The stain and photoetched PSi films have been suggested as being similar in nature to the anodically etched PSi films.[4–12]

The purpose of this article is to make clear the optical properties of PSi photoetched in aqueous HF/I_2 solution. To study the nanostructure properties of PSi, we perform spectroellipsometry (SE), electroreflectance (ER), photovoltage (PV), photoconductivity (PC), and Fourier transform infrared (FTIR) spectroscopy measurements. The quantum size or nanostructure effect considered here makes possible the quasidirect optical transitions in nanocrystallites via a relaxation of the momentum conservation at and above the indirect band edge, resulting in a supra-indirect-gap absorption and emission at ~2 (E_g^X) or ~2.5 eV (E_g^L). These results support the hypothesis that the visible light emission in PSi is based on surface-sensitive quantum confinement effect in Si nanocrystallites.

II. EXPERIMENT

The wafers used were *n*-type Si(100) with a resistivity of 1–3 Ω cm. They were first degreased using organic solvents in an ultrasonic bath, rinsed with deionized (DI) water, etched in 50% HF solution for 1 h, and rinsed in DI water. Before photoetching, the wafers were chemically cleaned in a sulfuric peroxide mixture (SPM) at ~80 °C for 5 min, followed by etching of chemical oxides in 50% HF solution for 1.5 h and rinsing with DI water. The SPM cleaning made to stably and uniformly form PSi on the light irradiated surfaces.[13] Photoetching was then performed by illuminating a 300 W Xe lamp onto the surfaces in a saturated solution of I_2 in 50% HF (see details in Ref. 11). After photoetching,

they were rinsed with DI water. The thickness of the PSi film was ~360 nm determined using a Talystep profilometer after a part of the film was removed by 2% NaOH solution.

The SE instrument was of the rotating-analyzer type (DVA-36VW-A, Mizojiri Optical, Co., Ltd.). The SE data were measured at room temperature in the 1.2–5.2 eV photon energy range with the angles of incidence 70° and polarizer azimuth 45°, respectively. PL measurements were performed at room temperature using a grating spectrometer (JASCO CT-25C) and a Peltier-device-cooled photomultiplier tube (Hamamatsu R375). The 325 nm line of a He−Cd laser (Kimmon IK3302R-E) chopped at 328 Hz was used as the excitation light source. The PL emission from crystalline silicon (*c*-Si) was also recorded using the 488 nm line of an Ar^+ laser as the excitation light source and a liquid-N_2-cooled Ge photodiode (Hamamatsu B6175–05) at room temperature.

In fabricating ER, PV, and PC devices, the reverse side of the wafer was first soldered by In electrode. Then, a semitransparent Au contact, 10 nm in thickness, was deposited by vacuum evaporation onto the PSi layer. Finally, the Au lead wires were taken from these electrodes. The ER measurements were performed at a bias voltage of −3 V with a modulation voltage of ±1 V. A lock-in-amp detection method was used to obtain ER, PV, and PC spectra. A 50 W tungsten lamp was used as the white light source. All the ER, PV, and PC spectra were recorded at room temperature using a grating spectrometer (JASCO CT-25C) and a Peltier-device-cooled photomultiplier tube (Hamamatsu R375).

The surface chemistry of the PSi samples was monitored by FTIR. The FTIR spectra were recorded in transmission mode at room temperature using a Nicolet Magna 560 spectrometer in the 400−2300 cm^{-1}. All the FTIR spectra were recorded with a resolution of 4 cm^{-1} using room air data as a reference.

III. RESULTS

A. SE measurement

Optical spectroscopy in the visible and UV regions has been an important tool in the investigation of electronic energy-band structure, as optical transitions can contribute as significant structures to the dielectric functions and their related optical spectra.[14] We used SE to study the relation between the structural and optical properties of *c*-Si and PSi materials. In Fig. 1(a), we show the experimental dielectric-function spectrum $\varepsilon(E)=\varepsilon_1(E)+i\varepsilon_2(E)$ for *c*-Si. The dominant peaks found in Fig. 1(a) are due to the E_1 and E_2 transitions.[15,16]

The E_1 transitions in *c*-Si take place along the ⟨111⟩ directions of the Brillouin zone ($\Lambda_3^v \rightarrow \Lambda_1^c$). Note that the lowest direct gap in *c*-Si corresponds to the E_0' transitions taking place at the Γ point, $\Gamma_{25'}^v \rightarrow \Gamma_{15}^c$. These transitions are nearly degenerate with the E_1 transitions. The spin−orbit splitting energies, Δ_0, Δ_0', and Δ_1, in Si are very small and are usually not clearly resolved in optical spectra of this material.[16]

The more pronounced structure found in *c*-Si at energies higher than E_1 is labeled E_2.[15,16] The nature of the E_2 transitions in Si is more complicated, as it does not correspond to a single, well-defined critical point (CP). Indeed, the precise low-filed ER analysis[17] revealed that the structure consists of three CPs, $E_2(1)$, $E_2(2)$, and $E_2(3)$, of type M_1, M_1, and M_2, respectively. The degenerating nature of the $E_2(1)$ and $E_2(2)$ CPs are due to an accidental coincidence of the M_1 saddle point in the ⟨110⟩ directions ($\Sigma_2^v \rightarrow \Sigma_3^c$) and an M_2 saddle point near the *X* point ($X_4^v \rightarrow X_1^c$).

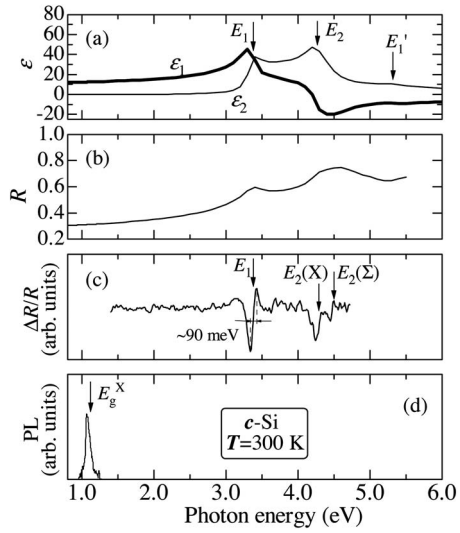

FIG. 1. ε, *R*, Δ*R*/*R*, and PL spectra of *c*-Si sample at *T*=300 K.

Plotted in Fig. 1(b) is the normal-incidence reflectivity spectrum *R* for *c*-Si obtained from the experimental $\varepsilon(E)$ data using

$$R=\frac{(\varepsilon_1^2+\varepsilon_2^2)^{1/2}-[2\varepsilon_1+2(\varepsilon_1^2+\varepsilon_2^2)^{1/2}]^{1/2}+1}{(\varepsilon_1^2+\varepsilon_2^2)^{1/2}+[2\varepsilon_1+2(\varepsilon_1^2+\varepsilon_2^2)^{1/2}]^{1/2}+1}. \quad (1)$$

The dominant peaks seen in Fig. 1(b) are due to the E_1 and E_2 transitions.

The corresponding SE $\varepsilon(E)$ and *R* data for our PSi sample are shown in Figs. 2(a) and 2(b), respectively. It is evident from Fig. 2(a) that the PSi $\varepsilon(E)$ spectrum is quite different from that of *c*-Si [Fig. 1(a)]. The weakened ε nature in the PSi sample is due to a density deficit, i.e., the presence

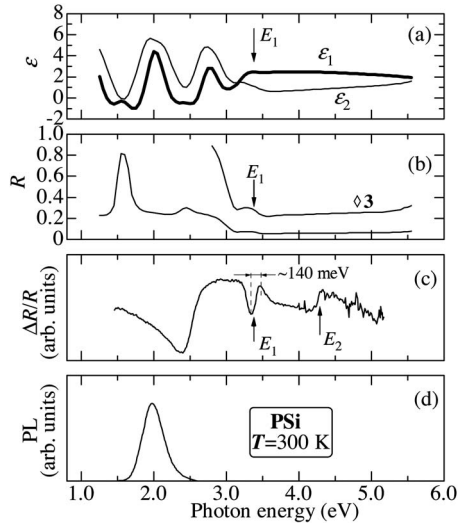

FIG. 2. ε, *R*, Δ*R*/*R*, and PL spectra of PSi sample at *T*=300 K.

of voids in the PSi layer. The large peaks both in ε_1 and ε_2 for $E \leq 3$ eV originate from a multiple internal reflection in the PSi layer where the material is nearly transparent. The E_1 structure can also be easily identified as a weak, but clear peak in the R spectrum at $E \sim 3.3$ eV. Note that R values (~ 0.1) for $E \geq 3$ eV in PSi are much smaller than those in c-Si. The Bruggeman effective medium approximation[14] suggests that the porosity of our PSi sample ($R \sim 0.1$) is approximately 70%.

B. ER measurement

ER technique can strongly enhance the changes in reflectivity R. The effect on R of the changes $\Delta\varepsilon_1$ and $\Delta\varepsilon_2$ induced by an external modulation parameter (M) can be given by[18]

$$\frac{\Delta R}{R} = \alpha \Delta\varepsilon_1 + \beta \Delta\varepsilon_2, \tag{2}$$

where the fractional coefficients α and β are functions of the photon energy E and their sign and relative magnitude determine the results of analysis in the different spectral regions.[18] In ER, the modulating electric field $M = \xi$ destroys the translational symmetry and then the low-field ER spectrum can be related to the third derivative of ε:

$$\Delta\varepsilon = \frac{(\hbar\Omega)^3}{3E^2} \frac{d^3}{dE^3}(E^2\varepsilon), \tag{3}$$

with

$$(\hbar\Omega)^3 = e^2\hbar^2\xi^2/8\mu, \tag{4}$$

where μ is the reduced interband effective mass. The third-derivative nature represented by Eq. (3) is the reason why ER spectrum is sharper and more richly structured than the conventional reflectivity spectrum R.

The experimental ER spectra for c-Si and PSi are shown in Figs. 1(c) and 2(c), respectively. In Fig. 1(c), the bulk c-Si sample has at least three CPs, $E_1 \sim 3.4$ eV, $E_2(X) \sim 4.3$ eV, and $E_2(\Sigma) \sim 4.5$ eV. There is no additional structure in Fig. 1(c), particularly for $E \leq 3$ eV where no strong optical transitions occur at the indirect absorption edges $E_g^X(\Gamma^v \rightarrow X^c)$ and $E_g^L(\Gamma^v \rightarrow L^c)$.

In Fig. 2(c), the PSi spectrum reveals the E_1 and E_2 structures at ~ 3.4 and ~ 4.3 eV, respectively. However, these structures are much broader than those in c-Si. For example, the E_1 structure width for c-Si is ~ 90 meV, whereas that for PSi is ~ 140 meV [cf. Figs. 1(c) and 2(c)]. The most noticeable feature found in the PSi spectrum is the appearance of the broad peak at energies below the lowest direct gap E_1 (≤ 3 eV). The ER studies on anodic PSi samples have also been extensively carried out by Toyama and Okamoto.[19–21] Their measured linearly polarized ER spectra suggest three main structures at ~ 1.3, $\sim 1.5-2.2$, and $\sim 2.3-2.7$ eV in glancing-angle incident geometry. These structures are considered to arise from the optical transitions associated with the confined electron–hole pairs in Si nanocrystallites. Note that our observed ER structure at ~ 2.5 eV resembles that obtained by Toyama *et al.* ($\sim 2.3-2.7$ eV).[21]

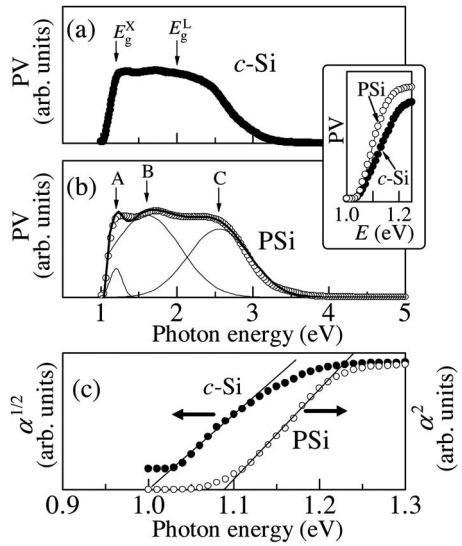

FIG. 3. PV spectra for (a) Au/n-Si Schottky and (b) Au/n-PSi/n-Si devices. The light solid lines in (b) represent the deconvolution of the experimental PV spectrum into several Gaussian peaks. (c) $\alpha^{1/m}$ vs E are plotted for c-Si ($m=2$) and PSi ($m=1/2$). The E_g values obtained in (c) are ~ 1.00 and ~ 1.09 eV for c-Si and PSi, respectively.

C. PV and PC measurements

PV and PC are important techniques for the study of photogenerated carrier transport properties and also of carrier recombination mechanisms in semiconductors. There have been many reports on the PV and PC properties of anodic PSi samples.[22–34] However, no study has been carried out on photoetched porous materials up to date.

We present in Figs. 3(a) and 3(b) our measured PV spectra for Au/n-type Si Schottky and Au/n-type PSi/n-type Si devices, respectively. In Fig. 3(a), the Au/n-Si Schottky device shows a weak maximum at ~ 1.2 eV(E_g^X) and a plateau-like sensitivity for $E \geq 1.2$ eV. This spectral feature is similar to those of commercial Si photodiodes. The Au/n-PSi/n-Si device, on the other hand, provides three individual peaks at ~ 1.2 (A), ~ 1.6 (B), and ~ 2.6 eV (C).

By performing Gaussian line-shape fit, our measured PV spectrum can be resolved into several peaks. The results of this fit are shown in Fig. 3(b) by heavy and light solid lines. The lowest peak at ~ 1.2 eV is nearly the same as that labeled E_g^X in Fig. 3(a). It should be noted, however, that the fundamental absorption edge observed in the Au/n-PSi/n-Si device is steeper than that in the Au/n-Si Schottky device, as clearly seen in the inset of Fig. 3.

Optical absorption coefficient α in the interband transition region is dependent on photon energy E approximately as[35]

$$\alpha \propto (E - E_g)^m, \tag{5}$$

where E_g is the band-gap energy and m is dependent on various interband transition processes, i.e., $m=1/2$ for dipole-allowed direct transitions, $m=3/2$ for dipole-forbidden direct transitions, $m=2$ for dipole-allowed indirect transitions, and $m=3$ for dipole-forbidden indirect transitions. Note that steep optical absorption is a characteristic of $m=1/2$. In Fig. 3(c), we plot $\alpha^{1/m}$ versus E for c-Si ($m=2$)

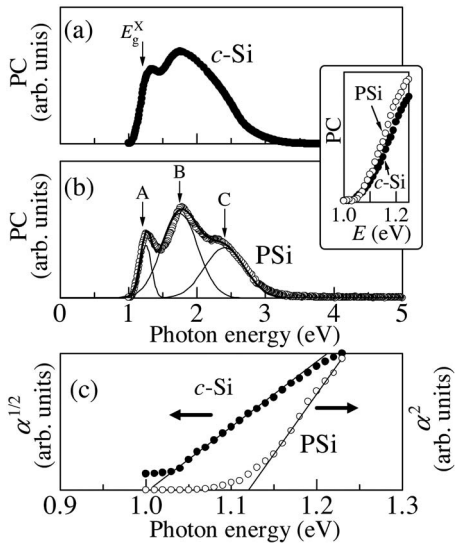

FIG. 4. PC spectra for (a) Au/*n*-Si Schottky and (b) Au/*n*-PSi/*n*-Si devices, The light solid lines in (b) represent the deconvolution of the experimental PC spectrum into several Gaussian peaks. (c) $\alpha^{1/m}$ vs E are plotted for *c*-Si ($m=2$) and PSi ($m=1/2$). The E_g values obtained in (c) are ~1.00 and ~1.12 eV for *c*-Si and PSi, respectively.

and PSi samples ($m=1/2$), respectively. Here, we simply assumed that our obtained PV signal is proportional to α. As expected, the fundamental absorption edge of *c*-Si is a dipole-allowed indirect band gap ($m=2$), whereas that of PSi is well fit by assuming $m=1/2$. As we will see later (Sec. IV), the absorption mechanism of $m=1/2$ observed in PSi is considered to be due to the quasidirect transitions at the nanocrystalline band gap. The E_g values obtained in Fig. 3(c) are ~1.00 eV (*c*-Si) and ~1.09 eV (PSi), respectively.

The full width at half maximum (FWHM) values of peaks *B* at ~1.6 eV and *C* at ~2.6 eV are about 1 eV. These peaks can be considered to stem from the PSi layer itself, but not from the bulk *n*-type silicon substrate. Indeed, such broader peaks have been sometimes observed in the 1–3 eV region of PV and PC spectra of anodically and stain-etched PSi devices.[22–34]

The same analysis results, but for PC spectra obtained at the $V=-1$ V biased condition, are shown in Fig. 4. All the peaks identified in the PV spectra can be clearly found in the PC spectra. The band-gap and peak energies fit determined in Fig. 4 are $E_g^X \sim 1.00$ eV (*c*-Si), $E_g^X \sim 1.12$ eV (PSi), ~1.75 eV (*B* peak), and ~2.40 eV (*C* peak), respectively. The blueshift in the fundamental absorption edge E_g^X of PSi from *c*-Si value has also been confirmed in the PC spectra [Fig. 4(c)].

D. PL measurement

Figures 1(d) and 2(d) show the room-temperature PL spectra obtained for *c*-Si and PSi samples, respectively. Because of lower luminescence efficiencies and higher absorption coefficients, no stronger PL has usually been observed in *c*-Si at or above the fundamental absorption edge. Indeed, our observed *c*-Si spectrum gives only a weak PL peak at ~1.1 eV, just below the lowest indirect absorption edge E_g^X [Fig. 1(d)]. The PSi sample, on the other hand, provides a PL

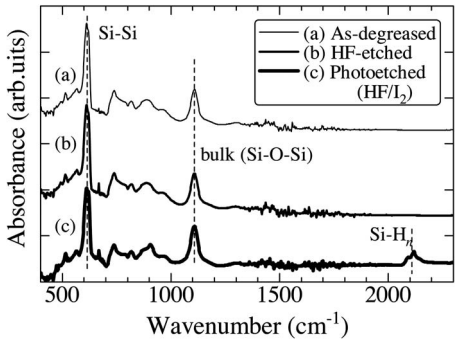

FIG. 5. FTIR spectra of (a) as-degreased *c*-Si, (b) HF-etched *c*-Si, and (c) HF/I_2-prepared PSi samples.

emission at ~2.0 eV [Fig. 2(d)]. The FWHM of this PL peak is about 0.4 eV. The PL peak is also found to locate in energy slightly smaller than that obtained in the ER spectrum ~2.5 eV [Fig. 2(c)]. As we discuss in Sec. IV, the mechanism of the PL emission is considered to be due to the supra-E_g^X emission, characteristic of nanocrystalline or porous materials.

E. FTIR measurement

To further survey the properties of photoetched PSi, we carried out FTIR measurements at room temperature. The results of (a) as-degreased *c*-Si, (b) HF-etched *c*-Si, and (c) HF/I_2-prepared PSi for $t=10$ min are shown in Fig. 5. The FTIR spectrum of the as-degreased *c*-Si sample exhibits strong absorption bands near 614 and 1107 cm^{-1} [Fig. 5(a)]. The most distinct peak at ~614 cm^{-1} is assigned to the summation band of the transverse optical and transverse acoustic phonons at the *X* (610.6 cm^{-1}) or *L* (603.9 cm^{-1}) point.[36] The relatively distinct peak at ~1107 cm^{-1} may also be due to a multiphonon band.[36] Note, however, that the 1040–1240 cm^{-1} spectral region is largely obscured by residual impurities. In fact, the peak at ~1107 cm^{-1} has been assigned to the bulk Si–O–Si mode.[37,38] Several FTIR peaks are also observed at around 2100 cm^{-1} on the HF/I_2-etched surface. These peaks correspond to the Si–H_n stretching modes at ~2090 (Si–H_2), ~2100 (Si–H_2), and ~2140 cm^{-1} (Si–H_3), respectively.

It is interesting to point out that no clear difference in the FTIR spectra can be found in Fig. 5 between the as-degreased (or HF-etched *c*-Si) and photoetched PSi samples. It means that the light emission in porous materials, at least in the HF/I_2-prepared samples, are not caused by any extrinsic origins or effects, such as hydrogenated amorphous Si, surface hydrides, defects in Si or SiO_x, siloxene, or surface states.[1,3]

We compare in Fig. 6 the FTIR spectrum of HF/I_2-prepared PSi sample to those obtained from samples photoetched in some HF/KIO_3 (Ref. 10) and HF/$FeCl_3$ mixed solutions (Ref. 12). As mentioned previously, we cannot find any characteristic PSi feature in the FTIR spectra of the HF/I_2-etched sample. We can see, however, a weak absorption shoulder in the HF/KIO_3-prepared PSi sample at ~1064 cm^{-1} [Fig. 6(b)]. It is assigned to the surface Si–O–Si stretching mode ν(Si–O–Si).[36]

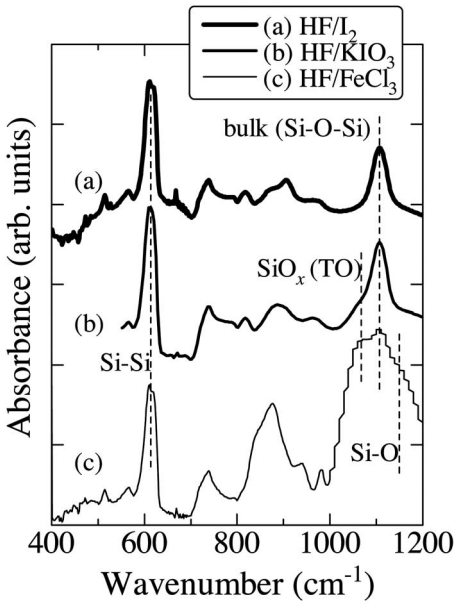

FIG. 6. FTIR spectra of PSi samples photoetched in (a) HF/I_2, (b) HF/KIO_3 (Ref. 10), and $HF/FeCl_3$ solutions (Ref. 12).

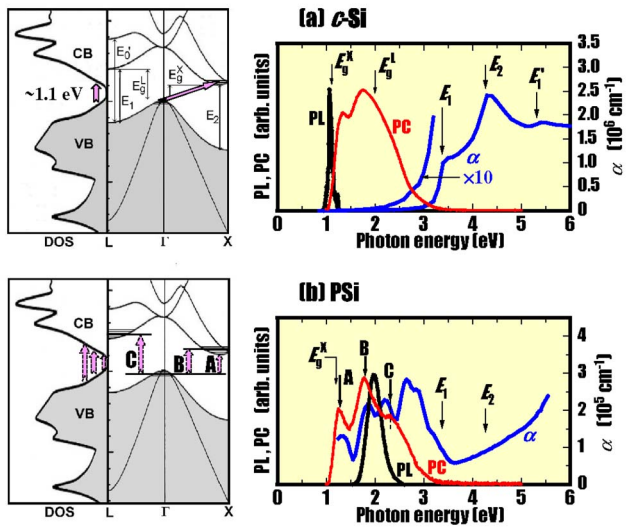

FIG. 7. (Color online) Electronic energy-band structure and density of state at the conduction (CB) and valence bands (VB), together with experimental PL, PC, and $\alpha(E)$ spectra for (a) *c*-Si and (b) PSi sample photoetched in HF/I_2 solution.

The FTIR spectrum of the $HF/FeCl_3$ sample in Fig. 6(c) exhibits the strong absorption peak at $\sim 1107\ \mathrm{cm}^{-1}$, together with several absorption shoulders at ~ 1067 and $\sim 1150\ \mathrm{cm}^{-1}$. These absorption shoulders grew large as the photoetching time t increased. The absorption at ~ 1067 and $\sim 1150\ \mathrm{cm}^{-1}$ can be assigned to the transverse optical phonons in thin SiO_x layer and to the Si–O stretching mode, respectively.

IV. DISCUSSION

A. Interference oscillation

There have been many reports on PSi formation by photoetching under He−Ne laser illumination. An incoherent light source (Xe lamp) used in this study made possible a large ($>20\times 20\ \mathrm{mm}^2$), homogeneous PSi layer formation. Addition of oxidant I_2 in HF solution also made possible reproducible formation of PSi layers in very short time. The resultant large-area PSi samples enabled to determine the $\varepsilon(E)$ spectrum and its related optical constants by using SE. Note that the usual SE measurement requires surface area of larger than $5\times 5\ \mathrm{mm}^2$.

Figure 7 presents SE $\alpha(E)$ data, together with PC and PL spectra, obtained for *c*-Si and PSi samples. As seen in Figs. 1, 2, and 7, the optical spectra of PSi are quite different from those of *c*-Si. The weakened optical strength observed in the PSi sample is due to a density deficit. The effective medium approximation suggests porosity $\sim 70\%$ of our PSi sample.[14]

It is very difficult to determine the lowest indirect-gap energy in an indirect-gap semiconductor as in *c*-Si by SE. This is because of the very weak optical density at the lowest indirect gap of *c*-Si. Indeed, our measured SE spectra showed an interference oscillation at the PSi layer, i.e., between the PSi surface and *n*-Si substrate. Observation of an interference oscillation promises that the porous layer thickness is thin and the porous material is nearly transparent. The thickness of our studied PSi layer is $\sim 0.36\ \mu\mathrm{m}$. The absorption coefficient of *c*-Si is less than $1\times 10^5\ \mathrm{cm}^{-1}$ for $E<E_1$ and is on the order of $10^6\ \mathrm{cm}^{-1}$ for $E\geq E_1$ [Fig. 7(a)]. The absorption coefficient of our PSi sample is much less than $10^6\ \mathrm{cm}^{-1}$ even for $E\geq E_1$ [Fig. 7(b)]. The $1\times 10^5\ \mathrm{cm}^{-1}$ ($1\times 10^6\ \mathrm{cm}^{-1}$) absorption coefficient corresponds to the light penetration depth of $\alpha^{-1}\sim 1\ \mu\mathrm{m}$ ($\sim 0.1\ \mu\mathrm{m}$). Thus, the peaks in $\varepsilon(E)$ [Fig. 2(a)], $R(E)$ [Fig. 2(b)], and $\alpha(E)$ [Fig. 7(b)] for $E<3$ eV can be concluded to arise from the interference oscillations in the PSi layer. On the other hand, an interference oscillation cannot be principally expected on ER spectra, even if samples have epitaxial layers or any quantum structures, such as quantum wells and superlattices. Similarly, interference oscillation has never been found in neither PV nor PC spectrum up to date.

It should be noted that the multiple interference oscillation is often observed in PL spectra of PSi samples. We show in Fig. 8(a), as an example, PL spectra for anodic PSi samples measured at 300 K. Here, the anodization was carried out on *p*-type Si(100) substrates with a resistivity of $10-15\ \Omega\ \mathrm{cm}$ in a HF/C_2H_5OH solution at $10\ \mathrm{mA/cm}^2$ for $t=1$, 3, 5, and 10 min. The corresponding SE $\varepsilon(E)$ spectra for $t=5$ min are plotted in Fig. 8(b).

In Fig. 8(a), the interference oscillations can be clearly seen for the anodic PSi samples for $t=3$ and 5 min. The oscillations in the SE $\varepsilon(E)$ data [Fig. 8(b)] have the same pitch in wavelength as in Fig. 8(a). However, no interference oscillation has been observed in neither PL nor $\varepsilon(E)$ spectra of the $t=1$ and 10 min samples. It should be noted that the interference oscillations were observed not only in anodic PSi samples but also in another nanocrystallite materials and amorphous Si films.[39–41] As the layer thickness $\sim 0.36\ \mu\mathrm{m}$ of our studied PSi sample is much smaller than that for the $t=3$ min anodic sample ($>1\ \mu\mathrm{m}$) in Fig. 8, we never observe an interference oscillation in our PL spectrum [see Fig. 2(d)].

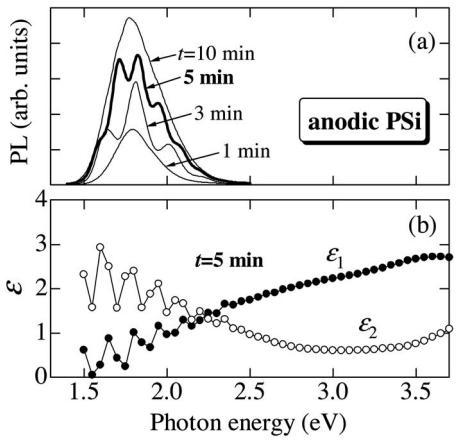

FIG. 8. (a) Room-temperature PL spectra for anodic PSi samples formed in a HF/C_2H_5OH solution for $t=1$, 3, 5, and 10 min. (b) SE $\varepsilon(E)$ spectra for anodic PSi sample formed in a HF/C_2H_5OH solution at 10 mA/cm^2 for $t=5$ min.

B. PV, PC, and ER spectra

Figure 9 shows a schematic representation of the energy-band diagram of our prepared PV device. Note that the PV device shown in Fig. 9 involves two junctions connected to each other in series: a "Schottky junction" between the transparent Au metal and *n*-PSi and a "heterojunction" between the *n*-PSi and *n*-Si substrate. Therefore, the PV effect can be considered as arising from both junctions as well as from optical absorption in the PSi layer itself. For comparison, we fabricated a Au/*n*-Si Schottky device by directly evaporating semitransparent Au film on the *n*-Si substrate. These two devices showed a clear rectifying behavior in the $I-V$ characteristics.

The highest PV and PC photoresponses in the 1−2 eV spectral region can be considered to stem from the Au/*n*-PSi Schottky junction and the *n*-PSi layer itself. Because of the large absorption coefficients for $E>3$ eV, no PV or PC signal can be observed in the region above $E_1\sim3.4$ eV (Figs. 3 and 4). Using a 100 W Xe lamp, instead of the 50 W tungsten lamp, we observed the PV signal up to 4.5 eV. Figure 10 shows the result of this experiment. Many fine structures seen in the ~2.5 eV region and below ~2 eV correspond to the xenon line spectra. As in Figs. 3 and 4, peaks *B* (~1.7 eV) and *C* (~2.5 eV) can be identified in the PV spectrum of the Au/*n*-PSi/*n*-Si device. Further, the E_1-related structure can be found at $E\sim3.5$ eV. Neither such a peak nor a structure can be observed in the Au/*n*-Si Schottky device spectrum. From a technological point of view, it is interesting to point out that the photosensitivity of the Au/*n*-PSi/*n*-Si device shifts to the higher energy range up to ~4.5 eV, promising it as future high-performance photonic devices.

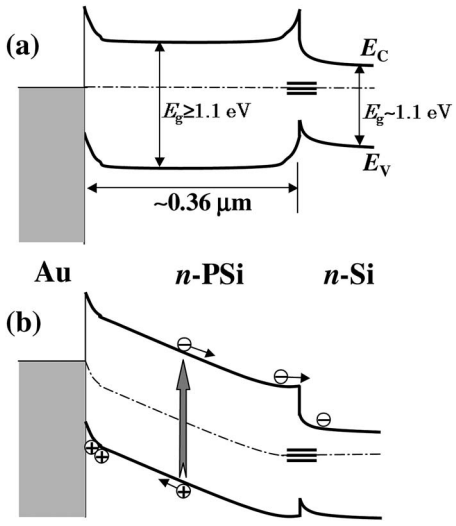

FIG. 9. Energy-band diagram of a Au/*n*-PSi/*n*-Si PV device at (a) open-circuit and (b) reverse-biased conditions.

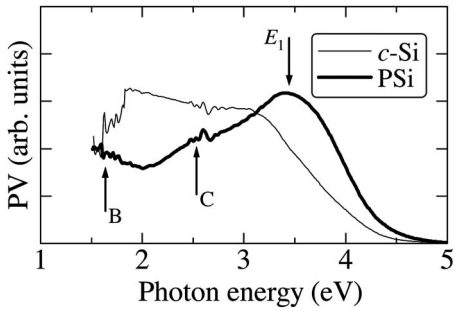

FIG. 10. PV spectra for Au/*n*-Si Schottky and Au/*n*-PSi/*n*-Si devices measured at the open-circuit condition using a Xe lamp, instead of a tungsten lamp. The fine structures seen in the ~2.5 eV region and below ~2 eV correspond to the xenon line spectra.

At the open-circuit condition [Fig. 9(a)], photoexcited carriers especially holes in the *n*-PSi layer have a chance of contribution to the PV effect. As the reverse bias increases, the Au/*n*-Si Schottky device has the dominant contribution to the PC effect. In Fig. 9(b), the photoexcited holes and electrons drift into the opposite directions. Because of the appropriate light penetration depth $\alpha^{-1}\sim1$ μm [$\alpha\sim1\times10^5$ cm^{-1}, see Fig. 8(b)], we can expect an efficient absorption of the light in the PSi layer, resulting in the observation of peaks *B* and *C* in the PSi layer [Fig. 4(b)].

The change in the lowest indirect gap E_g^X ($m=2$) to the lowest quasidirect gap ($m=1/2$) observed in Figs. 3 and 4 may be due to nanocrystallization-enhanced relaxation of the momentum conservation at the lowest absorption edge E_g^X in the PSi layer. It is well known that nanocrystallization leads to its electronic states blue-shifted. Indeed, the E_g^X energy (peak *A*) in Figs. 3 and 4 slightly blue-shifted from ~1.0 eV (*c*-Si) to ~1.1 eV (PSi), supporting an appearance of the quantum size effect. The smaller blueshifted value observed in PSi may be due to the larger electron and hole effective masses in the *X* minima and Γ maximum, respectively.[35]

In $\Delta R/R$ spectra, we observed only the single, broad peak at ~2.5 eV as the porous originated peak. On the other hand, Toyama and Okamoto[42,43] observed a few sharp ER peaks in anodic PSi samples, which were considered to be due to the optical transitions associated with the confined electron−hole pairs in the sample, together with a very broad peak at ~2.5 eV.[19–21] However, such "sharp" peaks were not observed in their measured PL emission spectra. We consider that the broad E_1 peak seen in Fig. 2(c) is also as a result of the nanocrystallite-induced broadening of the E_1 CP in the porous sample.

C. Supra-E_g^X emission

As the PSi nanocrystalline size observed by atomic force microscopy (AFM) is of the order of 20–100 nm,[10,44] we adopt a concept of the Brillouin zone not only about *c*-Si but also about PSi. The corresponding energy-band structures and density-of-states spectra are schematically shown on the left-hand side of Fig. 7.

In *c*-Si [Fig. 7(a)], the fundamental absorption edge corresponds to the indirect optical transitions from the highest valence band at the Γ point to the lowest conduction band near *X*. The direct optical transitions at or near *L*, *X*, and Γ have also been observed as the E_1, E_2, and E_0' CPs in optical spectra of *c*-Si. Note that the CPs in *c*-Si are primarily a result of the Bragg gaps at the Brillouin-zone boundaries, i.e., a consequence of the long-range order.

If the nanocrystalline size is actually on the order of 20–100 nm, we cannot expect a large energy shift of the quantum states enabling visible light emission from the PSi material. It should be noted, however, that a careful study is needed to determine nanocrystalline sizes as small as 10 nm.[1] It is, thus, proposed that the porous surfaces have a "fractal-type" morphology.[45] The AFM equipment used had silicon tips on 125-μm-wide-legged cantilever and tip radii in the range of 10–20 nm.[10,43] As the porous sizes are comparable to the tip radii, those radii should be taken as upper limits of the AFM true value.

Let us suppose that the supra-E_g^X emission observed at ~2 eV in PSi is a result of the quantum confinement in the PSi nanocrystallites. The indirect transitions in *c*-Si can be interpreted by the second-order perturbation, whereas the direct transitions are a first-order perturbation process. The higher order process at the indirect absorption edge is a result of the requirement of momentum conservation with emitting and/or absorbing phonons. Therefore, the transition probability is usually much smaller at the indirect absorption edge than at the direct edge.

It is possible to consider that the ~2 eV PL emission observed in PSi is due to nanocrystallite-enhanced relaxation of the momentum conservation at and above the lowest absorption edge E_g^X in the PSi layer [Fig. 7(b)]. The absence of long-range order in an amorphous material renders the Bloch theorem inapplicable and leaves the crystalline momentum $\hbar\mathbf{k}$ undefined. The optical transitions in such case can be described, to a first approximation, by the "quasidirect" or "nondirect" transition model in which conservation of the energy, but not the wave vector, is significant.[46,47] The resulting optical transitions provide a single, broad emission or absorption band in optical spectra, as typically observed in amorphous materials.[48] Thus, the quantum confinement effect considered here makes possible the quasidirect transitions at and above the indirect absorption edge, where many electronic states participated in the quasidirect transitions [Fig. 7(b)] may arise from the enhanced momentum fluctuation $\Delta\mathbf{k}$ due to the uncertainty principle in nanocrystallites. Similarly, ultrathin Si(100) film with thickness of d ~1.3 nm on a silicon-on-insulator substrate emitted light at ~1.46 eV and considered its emission mechanism as the quasidirect transitions caused by the quantum-mechanical momentum relaxation.[49]

Toyama *et al.*[50] also observed the direct-gap-like ER signals at ~1.20–1.37 eV arising from the fundamental absorption edge E_g^X of Si nanocrystallites deposited on glass substrates by radio frequency (rf) plasma chemical vapor deposition. They observed that by decreasing the mean crystallite size from ~3 nm to below 2 nm the fundamental energy gap is increased, i.e., blueshifted, and the $\Delta R/R$ signal is intensified. They considered that the increase in the E_g^X energy is due to the quantum confinement in Si nanocrystallites and the increased $\Delta R/R$ intensity as a result of the direct optical transitions. Some reports[51–53] also support the possibility of the quasidirect transitions in PSi.

The previous discussion promises that the ~2 eV peak observed in the PL spectrum is due to the supra-E_g^X emission. Peak *B* observed in the PC and PV spectra may also be caused by the supra-E_g^X absorption in the PSi sample. On the other hand, peak *C* seen both in the PC and PV spectra can be considered to be due to the supra-E_g^L absorption where it occurs between the filled Γ-valence and empty *L*-conduction bands in the first Brillouin zone [see Fig. 7(b)]. The large, broad peak observed at ~2.5 eV in the $\Delta R/R$ spectrum [Fig. 2(c)] may be due to the combined effect of the supra-E_g^X and supra-E_g^L absorptions in the PSi layer. The supra-E_g^X emission has also been clearly observed in anodic porous GaP sample.[54]

We show in Fig. 6 the FTIR results obtained from PSi samples formed in HF/I_2, HF/KIO_3, and $HF/FeCl_3$ solutions. The order of the PL intensity we obtained was $PSi(HF/I_2) > PSi(HF/FeCl_3) > PSi(HF/KIO_3)$. The main reason for this order is that the thicker PSi gives the stronger PL intensity.[10] Unlike anodic etching, photoetched PSi sample has a limited thickness value, ~400 nm in the present study (HF/I_2) and ~100 nm in Ref. 10 (HF/KIO_3), which may be determined by several factors, such as the solution composition and temperature. In stain-etched PSi, the limited thickness is determined by balancing of the Si dissolution rates of the bottom part and the top surface of the porous layer. The same mechanism as in stain etching can be easily expected in photoetching.

The enormous inner surface of PSi leads to the proposal that it is largely involved in the luminescence process. The surface recombination velocity is the only parameter required to characterize the surface.[55,56] The larger the surface recombination velocity, the smaller the minority carrier accumulation, or equivalently, the larger the surface recombination velocity, the weaker the PL intensity. The presence of surface oxide is expected to reduce the surface recombination velocity.[57]

It is noted that the HF/I_2-prepared PSi spectrum in Fig. 6 suggests no presence of surface oxides. This fact suggests that any surface oxide is not the origin of visible light emission in PSi materials. The strongest PL intensity observed in the HF/I_2 sample is, thus, considered to be due to an efficient surface passivation by atomic hydrogen (see Fig. 5). It is well known that the surface of freshly etched PSi is almost totally covered by SiH_x groups. The HF/KIO_3- and

$HF/FeCl_3$-prepared PSi samples also showed a great reduction in their PL intensities after passively etching the surface native oxide by aqueous HF solution. Further, the aged HF/I_2-prepared sample reduced its PL intensity by etching in aqueous HF solution. Thus, we consider that the yellow light emission observed in our PSi samples is due to surface-sensitive quantum confinement effect in silicon nanocrystallites. It is suggested that the surface oxide acts as a good passivation film and gives rise to an efficient emission at the PSi/oxide interface.[58] It should be noted, however, that it is difficult to establish a direct correlation between the visible luminescence properties in PSi and any particular chemical species or films on it.[59]

V. CONCLUSIONS

We investigated the optical properties of PSi photoetched in a HF/I_2 solution using various spectroscopic techniques. The addition of an oxidizing agent I_2 in HF and use of a incoherent light source (Xe lamp) made possible to obtain large, uniform PSi samples in very short time ($\leq$10 min). The SE $\varepsilon(E)$ and related optical spectra, such as $R(E)$ and $\alpha(E)$, showed an interference oscillation below $E \sim 3$ eV where the PSi sample is nearly transparent. The PV and PC spectra revealed three individual peaks at $\sim$1.2 (A), $\sim$1.7 (B), and $\sim$2.5 eV (C), in the almost transparent spectral region, i.e., below $\sim$3 eV, of the PSi sample. The ER spectrum provided peak, C, as a large, broad peak at $\sim$2.5 eV, together with a broadened peak E_1 at $\sim$3.4 eV. The room-temperature PL spectrum revealed a yellow emission centered at $\sim$2.0 eV. This emission corresponds to that found in the PV and PC spectra (peak B). As the PSi crystallite size determined by AFM was of the order of 20–100 nm, the porous sample was assumed to have the same energy-band diagram as that of the bulk crystalline Si. Then, absorption and/or emission peaks A, B, and C in the PSi spectra were considered to arise from the quasidirect transitions at and above the lowest absorption edges E_g^X (A and B) and E_g^L (C) in the PSi layer. The quantum-mechanical size effect, namely, a relaxation of the momentum conservation, made possible the quasidirect or nondirect optical transitions in such mesoscopic materials. Change in the optical transition nature from the indirect optical transitions characterized by an expression $\alpha \propto (E-E_g^X)^2$ in c-Si to the direct optical transitions given by $\alpha \propto (E-E_g^X)^{1/2}$ may be a result of the quasidirect transitions at the E_g^X edge in the PSi material. The FTIR data further suggested that the yellow light emission at $\sim$2.0 eV is due to the surface-sensitive quantum confinement effect, but is not originating from any extrinsic origins, such as surface hydrides or oxides.

ACKNOWLEDGMENTS

The authors would like to thank T. Miyazaki, S. Ozaki, and S. Tomioka for their experimental support and useful discussion.

[1] S. Ossicini, L. Pavesi, and F. Priolo, *Light Emitting Silicon for Microphotonics* (Springer, Berlin, 2003).
[2] L. T. Canham, Appl. Phys. Lett. **57**, 1046 (1990).
[3] A. G. Cullis, L. T. Canham, and P. D. J. Calcott, J. Appl. Phys. **82**, 909 (1997).
[4] J. Sarathy, S. Shih, K. Jung, C. Tsai, K.-H. Li, D.-L. Kwang, J. Campbell, S.-L. Yan, and A. J. Bard, Appl. Phys. Lett. **60**, 1532 (1992).
[5] N. Noguchi and I. Suemune, Appl. Phys. Lett. **62**, 1429 (1993).
[6] N. Yamamoto and H. Takai, Jpn. J. Appl. Phys., Part 1 **38**, 5706 (1999).
[7] N. Yamamoto and H. Takai, Thin Solid Films **359**, 184 (2000).
[8] L. Koker and K. W. Kolasinksi, J. Phys. Chem. B **105**, 3864 (2001).
[9] L. Koker and K. W. Kolasinksi, Phys. Chem. Chem. Phys. **2**, 277 (2000).
[10] Y. K. Xu and S. Adachi, J. Phys. D **39**, 4572 (2006).
[11] S. Adachi and T. Kubota, Electrochem. Solid-State Lett. **10**, H39 (2007).
[12] Y. K. Xu and S. Adachi, J. Appl. Phys. **101**, 103509 (2007).
[13] S. Tomioka, T. Miyazaki, and S. Adachi, Jpn. J. Appl. Phys., Part 1 **46**, 5021 (2007).
[14] See, for example, W. Theiß, Surf. Sci. Rep. **29**, 91 (1997).
[15] P. Lautenschlager, M. Garriga, L. Viña, and M. Cardona, Phys. Rev. B **36**, 4821 (1987).
[16] S. Adachi, Phys. Rev. B **38**, 12966 (1988).
[17] K. Kondo and A. Moritani, Phys. Rev. B **15**, 812 (1977).
[18] B. O. Seraphin and N. Bottka, Phys. Rev. **145**, 628 (1966).
[19] T. Toyama, A. Shimode, and H. Okamoto, Mater. Res. Soc. Symp. Proc. **609**, A24.10 (2000).
[20] T. Toyama, Y. Nakai, K. Moriguchi, and H. Okamoto, Phys. Status Solidi A **197**, 482 (2003).
[21] T. Toyama, Y. Nakai, K. Moriguchi, and H. Okamoto, Mater. Res. Soc. Symp. Proc. **737**, 499 (2000).
[22] J. P. Zheng, K. L. Jiao, W. P. Shen, W. A. Anderson, and H. S. Kwok, Appl. Phys. Lett. **61**, 459 (1992).
[23] C. Tsai, K.-H. Li, J. C. Campbell, and A. Tasch, Appl. Phys. Lett. **62**, 2818 (1993).
[24] P. Hlinomaz, O. Klíma, A. Hospodková, E. Hulicius, J. Oswald, E. Šípek, and J. Kočka, Appl. Phys. Lett. **64**, 3118 (1994).
[25] T. Ozaki, M. Araki, S. Yoshimura, H. Koyama, and N. Koshida, J. Appl. Phys. **76**, 1986 (1994).
[26] L. A. Balagurov, D. G. Yarkin, G. A. Petrovicheva, E. A. Petrova, A. F. Orlov, and S. Y. Andryushin, J. Appl. Phys. **82**, 4647 (1997).
[27] R. M. Mehra, V. Agarwal, V. K. Jain, and P. C. Mathur, Thin Solid Films **315**, 281 (1998).
[28] A. S. Dafinei and A. A. Dafinei, J. Non-Cryst. Solids **245**, 92 (1999).
[29] É. B. Kaganovich, É. G. Manoĭlov, and S. V. Svechnikov, Semiconductors **33**, 327 (1999).
[30] B. Ünal and S. C. Bayliss, J. Appl. Phys. **87**, 3547 (2000).
[31] G. Lérondel, F. Madéore, R. Romestain, and F. Muller, Thin Solid Films **366**, 216 (2000).
[32] B. Ünal, A. N. Parbukov, and S. C. Bayliss, Opt. Mater. **17**, 79 (2001).
[33] D. F. Timokhov and F. P. Timokhov, J. Phys. Stud. **8**, 173 (2004).
[34] T. V. Torchynska, A. V. Hernandez G. Polupan, S. J. Sandoval, M. E. Cueto, R. P. Sierra, and G. R. P. Rubio, Thin Solid Films **492**, 327 (2005).
[35] S. Adachi, *Properties of Group-IV, III–V and II–VI Semiconductors* (Wiley, Chichester, 2005).
[36] R. J. Collins and H. Y. Fan, Phys. Rev. **93**, 674 (1954).
[37] Z. Jichang, W. Jiangen, M. Bilan, Z. Jingbing, and Q. Fenyuan, Infrared Phys. **33**, 381 (1992).
[38] D. B. Mawhinney, J. A. Glass, Jr., and J. T. Yates, Jr., J. Phys. Chem. B **101**, 1202 (1997).
[39] D. C. Marra, E. Aydil, S.-J. Joo, E. Yoo, and V. I. Srdanov, Appl. Phys. Lett. **77**, 3346 (2000).
[40] S.-Y. Seo, K.-S. Cho, and J. H. Shin, Appl. Phys. Lett. **84**, 717 (2004).
[41] S. M. Orbons, M. G. Spooner, and R. G. Elliman, J. Appl. Phys. **96**, 4650 (2004).
[42] T. Toyama, Y. Nakai, and H. Okamoto, Mater. Res. Soc. Symp. Proc. **638**, F3.5 (2001).
[43] T. Toyama, Y. Nakai, A. Asano, and H. Okamoto, J. Non-Cryst. Solids **299–302**, 290 (2002).
[44] K. Uchida, K. Tomioka, and S. Adachi, J. Appl. Phys. **100**, 014301 (2006).
[45] T. George, M. S. Anderson, W. T. Pike, T. L. Lin, R. W. Fathauer, K. H. Jung, and D. L. Kwong, Appl. Phys. Lett. **60**, 2359 (1992).
[46] S. Adachi, H. Mori, and S. Ozaki, Phys. Rev. B **66**, 153201 (2002).
[47] D. T. Pierce and W. E. Spicer, Phys. Rev. B **5**, 3017 (1972).
[48] S. Adachi, Phys. Rev. B **43**, 12316 (1991).
[49] S. Saito, D. Hisamoto, H. Shimizu, H. Hamamura, R. Tsuchiya, Y. Matsui, T. Mine, T. Arai, N. Sugii, K. Torii, S. Kimura, and T. Onai, Jpn. J. Appl. Phys., Part 2 **45**, L679 (2006).
[50] T. Toyama, Y. Kotani, A. Shimode, and H. Okamoto, Appl. Phys. Lett. **74**,

3323 (1999).
[51]M. Rosenbauer, S. Finkbeiner, E. Bustarret, J. Weber, and M. Stutzmann, Phys. Rev. B **51**, 10539 (1995).
[52]M. Ben-Chorin, B. Averboukh, D. Kovalev, G. Polisski, and F. Koch, Phys. Rev. Lett. **77**, 763 (1996).
[53]G. Polisski, H. Heckier, D. Kovalev, M. Schwartzkopff, and F. Koch, Appl. Phys. Lett. **73**, 1107 (1998).
[54]K. Tomioka and S. Adachi, J. Appl. Phys. **98**, 073511 (2005).
[55]V. Grivickas, J. A. Tellefsen, and M. Willander, in *Properties of Crystalline Silicon*, edited by R. Hull (INSPEC, London, 1999), p. 718.
[56]J. Rappich and T. Dittrich, in *Thin Films*, edited by M. H. Francombe (Academic, San Diego, 2002), Vol. 29, p. 135.
[57]K. Tsunoda, E. Ohashi, and S. Adachi, J. Appl. Phys. **94**, 5613 (2003).
[58]T. Maruyama and S. Ohtani, Appl. Phys. Lett. **65**, 1346 (1994).
[59]S. Banerjee, K. L. Narasimhan, and A. Sardesai, Phys. Rev. B **49**, 2915 (1994).